Published for SISSA by Springer

Received: December 24, 2013
Accepted: February 14, 2014
Published: March 31, 2014

Electroweak $ZZjj$ production in the Standard Model and beyond in the POWHEG-BOX V2

Barbara Jäger,[a] **Alexander Karlberg**[b] **and Giulia Zanderighi**[b]

[a] *PRISMA Cluster of Excellence & Institute of Physics, Johannes Gutenberg University, 55099 Mainz, Germany*

[b] *Rudolf Peierls Centre for Theoretical Physics, 1 Keble Road, University of Oxford, U.K.*

E-mail: jaegerba@uni-mainz.de, alexander.karlberg@physics.ox.ac.uk, g.zanderighi1@physics.ox.ac.uk

Abstract: We present an implementation of electroweak $ZZjj$ production in the POWHEG BOX V2 framework, an upgrade of the POWHEG BOX program which includes a number of new features that are particularly helpful for high-multiplicity processes. We consider leptonic and semi-leptonic decay modes of the Z bosons, and take non-resonant contributions and spin correlations of the final-state particles into account. In the case of decays to leptons, we also include interactions beyond the Standard Model that arise from an effective Lagrangian which includes CP conserving and violating operators up to dimension six. We find that while leptonic distributions are very sensitive to anomalous couplings, because of the small cross-section involved, these analyses are feasible only after a high-luminosity upgrade of the LHC. We consider the cases of a 14 TeV, 33 TeV and 100 TeV machine and discuss the limits that can be placed on those couplings for different luminosities.

Keywords: Monte Carlo Simulations, NLO Computations

ArXiv ePrint: 1312.3252

doi:10.1007/JHEP03(2014)141

JHEP03(2014)141

Contents

1 Introduction

A primary goal of the CERN Large Hadron Collider (LHC) is an in-depth understanding of the mechanism responsible for electroweak symmetry breaking. Data collected and analyzed by the ATLAS [1] and CMS [2] collaborations have revealed the existence of a scalar boson with a mass of about 125 GeV. Investigations on the properties of this new particle consolidate its interpretation as the Higgs boson of the Standard Model (SM). In particular, measurements of its spin and CP properties [3, 4] as well as of its couplings to gauge bosons and fermions so far have disclosed no deviation from the SM expectation of a spin-zero, CP-even particle. Should physics beyond the Standard Model be realized in nature, its effects on observables in the Higgs sector seem to be small, calling for high precision in experiment as well as in theoretical predictions.

An ideal environment for the determination of the tensor structure and strengths of the Higgs couplings to gauge bosons is provided by vector-boson fusion (VBF) processes [5–7]. With their very pronounced signature in phase space, featuring two well-separated jets in the forward regions of the detector, VBF reactions can be separated well from QCD-induced background reactions.

In this work we wish to present a new tool for the simulation of Z-boson pair production via vector boson fusion. The purely electroweak process $pp \to ZZjj$ predominantly proceeds via the scattering of two quarks by the exchange of weak vector bosons in the t-channel with subsequent emission of two Z bosons. Diagrams with a Higgs resonance contribute as well as weak boson scattering graphs that are sensitive to triple and quartic gauge boson couplings.

The next-to-leading order (NLO) QCD corrections to this process, including leptonic decays of the Z bosons in the $\ell^+\ell^-\ell'^+\ell'^-$ and $\ell^+\ell^-\nu\bar{\nu}$ modes, have been computed in ref. [8] and are publicly available in the computer package `VBFNLO` [9–11]. While that code allows the computation of, in principle, arbitrary distributions within experimentally feasible selection cuts, an interface to parton-shower Monte Carlo programs at NLO-QCD

JHEP03(2014)141

accuracy is not yet available. We have therefore worked out a matching of the NLO-QCD calculation with parton-shower programs in the framework of the POWHEG formalism [12, 13], a method that allows to combine parton-level NLO-QCD expressions with a transverse-momentum ordered parton-shower in a well-defined manner. To this end, we are making use of the POWHEG BOX [14], a tool that provides all the process-independent building blocks of the matching procedure, but requires the user to implement process-specific ingredients in a specific format by himself. Recently a Version 2 of the POWHEG BOX has been released, POWHEG BOX V2. Version 2 includes a number of new features among which are

- the possibility to produce grids in parallel and combine them;
- the option to modify scales and parton distribution functions a posteriori, through a reweighting procedure of Les Houches events;
- a faster calculation of upper bounds, and the possibility to store upper bounds and combine them;
- an improvement in the separation of regions for the real radiation [15], which results in smoother distributions.

Given the complexity of electroweak $ZZjj$ production, we found it useful to take full advantage of these features and therefore implemented the process directly in Version 2 of the POWHEG BOX.

In the following section we describe the technical details of our implementation. In section 3 we present phenomenological results for some representative applications in the case of leptonic final states, in the case of cuts suitable to study the continuum, double-resonant production. We also discuss the potential of this process to constrain the size of dimension-six operators that arise in effective field theory approaches to physics beyond the Standard Model. In particular we study the capability of future colliders to constrain the couplings even further. We conclude in section 4.

2 Technical details of the implementation

Our implementation of electroweak $ZZjj$ production in the context of the POWHEG BOX proceeds along the same lines as previous work done for Zjj [16], W^+W^+jj [17], and W^+W^-jj production [18] via vector-boson fusion. We therefore refrain from a detailed description of technical aspects that are common to all vector-boson fusion processes considered so far, but refer the interested reader to the aforementioned references.

The first calculation of the NLO-QCD corrections to $ZZjj$ production via VBF in the context of the Standard Model, including decays of the Z-boson pair into four leptons or two leptons plus two neutrinos, has been presented in ref. [8] and is publicly available in the context of the VBFNLO package [9–11]. We adapted the matrix elements of that calculation to the format required by the POWHEG BOX, and additionally computed the scattering amplitudes for the semi-leptonic decay modes of the Z bosons.

JHEP03(2014)141

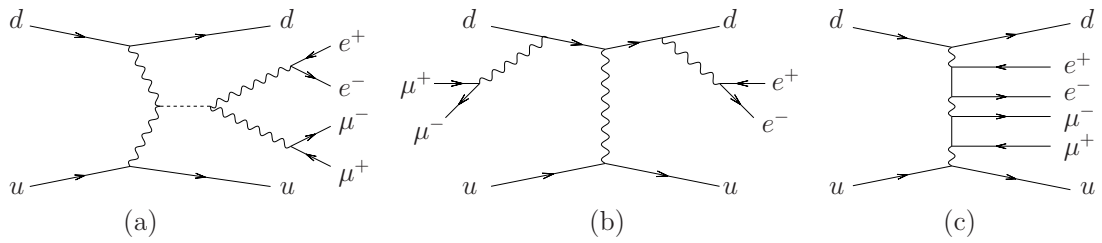

Figure 1. Representative Feynman diagrams for the partonic subprocess $ud \to e^+e^-\mu^+\mu^-ud$ at leading order.

In addition to that we account for physics beyond the Standard Model in the weak gauge boson sector by means of an effective field theory approach [19] with operators of dimension six that affect triple and quartic gauge boson vertices, but do not change the QCD structure of the Standard Model. Details of the operators entering the Lagrangian are given later. Notice that because decays are not affected by QCD corrections, it is enough to have a Leading Order (LO) implementation of the modified decay currents even at NLO in QCD. We could therefore adapt the LO implementation of the effective field theory in `MadGraph 5` [20] for the modeling of the modified electroweak building blocks needed for $pp \to ZZjj$.

In either model, at order $\mathcal{O}(\alpha^6)$ electroweak $ZZjj$ production predominantly proceeds via the scattering of two (anti-)quarks mediated by weak-boson exchange in the t-channel. The external Z bosons that in turn decay into a pair of leptons, neutrinos, or quarks can be emitted from either of the two fermion lines, or stem from vector-boson scattering sub-amplitudes of the type $VV \to VV$ (with V generically denoting a photon, a $W^\pm$, or a Z boson). In order to maintain electroweak gauge invariance, contributions with one or two photons instead of the Z bosons and diagrams for single- and non-resonant four-fermion production in association with two jets have to be considered as well. A representative set of diagrams is depicted in figure 1.

For partonic subprocesses with quarks of identical flavor, in addition to the afore-mentioned t-channel exchange diagrams, u-channel diagrams arise that are taken fully into account. However, the interference of u-channel with t-channel contributions is neglected. We furthermore disregard contributions induced by the exchange of a weak boson in the s-channel. This gauge-invariant subset of diagrams is strongly suppressed in the phase-space regions that are explored experimentally in vector-boson-fusion searches, cf. ref. [21] for a tree-level assessment of the numerical impact these contributions have in a realistic setup for the related case of electroweak W^+W^+jj production at the LHC.

For $\ell^+\ell^-\nu_\ell\bar{\nu}_\ell$ final states we neglect the interference with W^+W^-jj production, when the W bosons decay into the same final state. In the case of QCD production, this interference has been shown to be very small [22]. In the semi-leptonic decay modes, interference effects between the scattering quarks and the decay quarks are neglected.

For simplicity, we will refer to the electroweak production processes $pp \to \ell^+\ell^-\ell'^+\ell'^-jj$, $pp \to \ell^+\ell^-\nu\bar{\nu}jj$, and $pp \to \ell^+\ell^-\bar{q}qjj$ within the afore-mentioned approximations as $ZZjj$ production via VBF in the fully leptonic, leptonic-invisible and semi-leptonic decay modes,

JHEP03(2014)141

respectively, even though we always include contributions from off-resonant diagrams that do not arise from a $ZZjj$ intermediate state.

In the case of semi-leptonic decay modes we do not explicitly take into account QCD corrections to the hadronic decays of the Z bosons, or QCD corrections that connect the $ZZjj$ production with the $Z \to \bar{q}q$ decay processes. While the latter corrections are expected to be very small, corrections to the hadronic Z decay are well-described by Monte-Carlo programs that are interfaced to our NLO-QCD calculation. In fact their decay machinery is tuned to reproduce collider data.

We note that, similarly to the cases of electroweak Zjj and W^+W^-jj production, the `POWHEG BOX` requires a prescription for dealing with singularities emerging in the Born cross section for $pp \to ZZjj$ via VBF. One such type of singularities stems from collinear $q \to q\gamma$ configurations that emerge when a photon of low virtuality is exchanged in the t-channel. Phenomenologically, such contributions are irrelevant, as they are entirely removed once VBF-specific selection cuts are applied on the $ZZjj$ cross section that require the two partons of the underlying Born configuration to exhibit sufficient transverse momentum to be identified as tagging jets. We therefore drop this type of contributions already at generation level, by removing all events with an exchange boson in the t-channel with a virtuality smaller than $Q^2_{\rm min} = 4\ {\rm GeV}^2$. To improve the efficiency of the phase-space integration, we use a Born-suppression factor $F(\Phi_n)$ that dampens the phase-space integrand whenever a singular configuration is approached. This is ensured by the choice

$$F(\Phi_n) = \left(\frac{p_{T,1}^2}{p_{T,1}^2 + \Lambda^2}\right)^2 \left(\frac{p_{T,2}^2}{p_{T,2}^2 + \Lambda^2}\right)^2 , \tag{2.1}$$

where the $p_{T,i}$ denote the transverse momenta of the two final-state partons of the underlying Born configuration, and Λ is a cutoff parameter that we set to 10 GeV.

In VBF $ZZjj$ production processes, an additional type of singular configurations is caused by diagrams with a quasi on-shell photon that decays into a fermion pair, $\gamma^\star \to f\bar{f}$. Such contributions can easily be identified by a small value of the invariant mass m_{ff} of the decay system. In our simulations, we remove all configurations with $m_{ff} < m_{ff}^{\rm gen}$, where we set

$$m_{ff}^{\rm gen} = 20\ {\rm GeV}\,, \tag{2.2}$$

unless explicitly stated otherwise.

In the presence of a light Higgs boson, the VBF $ZZjj$ cross section receives contributions from two regions of phase space with very different kinematic properties. Therefore it is useful to split the phase space into two separate regions, around and away from the Higgs resonance. The full result is then obtained by adding the results of the two separate contributions [17].

3 Phenomenological results

We will concentrate in the following on the fully charged leptonic decay mode, which has a smaller branching fraction than the semi-leptonic ($\ell^+\ell^-\bar{q}q$) or the lepton-neutrino ($\ell^+\ell^-\nu\bar{\nu}$)

JHEP03(2014)141

decay modes, but is experimentally cleaner. Because of the Higgs and Z resonances, events tend to have either four leptons with an invariant mass close to the Higgs mass, or two pairs of leptons with an invariant mass close to the mass of the Z boson each. Typically, according to whether one is interested in studying Higgs production with subsequent $H \to ZZ^{(\star)}$ decays or VBF ZZ production in the continuum one applies different invariant mass cuts that suppress one of the two contributions, and leave the other almost unchanged. Continuum VBF ZZ production is a rare SM process that is well-suited to probe triple but also quartic gauge boson couplings. In this section we present few sample results obtained with our `POWHEG BOX` implementation, both in the pure SM and involving anomalous couplings that in our framework arise from an effective Lagrangian.

Let us stress here that the $\ell^+\ell^-\bar{q}q$ mode, although plagued by large QCD backgrounds, could in principle be studied with an analysis that uses boosted techniques and jet-substructure (see e.g. ref. [23]), along the lines of what was done in ref. [18]. However, because of the small production cross sections for VBF $ZZjj$, considering the boosted regime where only a tiny part of the inclusive cross section survives is pointless at the LHC.

3.1 Standard Model results

Anticipating the imminent energy upgrade of the LHC we consider proton-proton collisions at a center-of mass energy of $\sqrt{s} = 14\,\text{TeV}$. We use the NLO-QCD set of the MSTW2008 parametrization [24] for the parton distribution functions of the proton, as implemented in the `LHAPDF` library [25]. Jets are defined according to the anti-k_T algorithm [26, 27] with $R = 0.4$, making use of the `FASTJET` package [28]. Electroweak (EW) input parameters are set according to known experimental values and tree-level electroweak relations. As input we use the mass of the Z boson, $m_Z = 91.188\,\text{GeV}$, the mass of the W boson, $m_W = 80.419\,\text{GeV}$, and the Fermi constant, $G_F = 1.16639 \times 10^{-5}\,\text{GeV}^{-1}$. For the widths of the weak bosons we use $\Gamma_Z = 2.51\,\text{GeV}$ and $\Gamma_W = 2.099\,\text{GeV}$. The width of the Higgs boson is set to $\Gamma_H = 0.00498\,\text{GeV}$ which corresponds to $m_H = 125\,\text{GeV}$. Factorization and renormalization scales are set to $\mu_\text{F} = \mu_\text{R} = m_Z$ throughout, unless specified otherwise.

Here, we present numerical results for VBF $ZZjj$ production at the LHC in the fully leptonic decay mode. Our analysis requires each lepton pair to have an invariant mass close to m_Z. This completely excludes any contamination from a Higgs boson consistent with the one observed by the `ATLAS` and `CMS` collaborations at $m_H = 125\,\text{GeV}$ [1, 2], which results in $H \to ZZ^{(\star)}$ decays with at least one off-shell gauge boson. Our phenomenological study is inspired by [29]. In the following, we will always consider decays to $e^+e^-\mu^+\mu^-$. Neglecting same-type lepton interference effects, the cross-section for Z bosons decaying to any combination of electrons and muons is twice as large. In section 3.1 all results are quoted for the $pp \to e^+e^-\mu^+\mu^-jj$ decay mode only, whereas the results in section 3.2 have been obtained for the $pp \to e^+e^-\mu^+\mu^-jj$ decay mode and then multiplied by two to account for any decay into electrons or muons, while neglecting same-type lepton interference effects.

The VBF and invariant mass cuts that we apply in the following, inspired by refs. [30, 31], are very effective in suppressing QCD-like processes with colored objects in the t-

JHEP03(2014)141

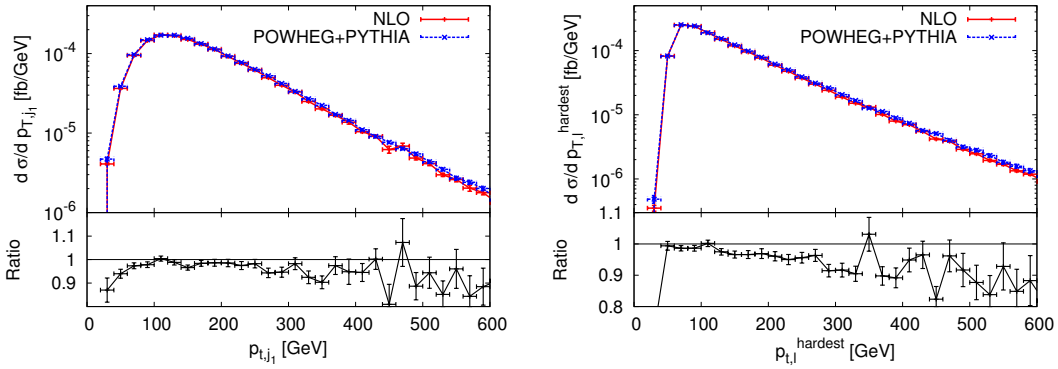

Figure 2. Transverse momentum distributions of the hardest jet (left) and the hardest lepton (right) for $pp \to e^+e^-\mu^+\mu^- jj$ at the LHC with $\sqrt{s} = 14$ TeV within the cuts of eqs. (3.1)–(3.5) at NLO (red) and NLO+PS (blue). The lower panel shows the ratio between NLO and NLO-PS.

channel. In particular, we require the presence of at least two jets with

$$p_{T,j} > 25 \text{ GeV}\,, \quad y_j < 4.5\,. \tag{3.1}$$

The two hardest jets satisfying these cuts are called "tagging jets" and are furthermore forced to be well separated by the VBF cuts

$$|y_{j_1} - y_{j_2}| > 4.0\,, \quad y_{j_1} \cdot y_{j_2} < 0\,, \quad m_{j_1 j_2} > 600 \text{ GeV}\,. \tag{3.2}$$

For the leptons we require

$$p_{T,\ell} > 25 \text{ GeV}\,, \quad y_\ell < 2.4\,, \quad R_{j\ell} > 0.4\,. \tag{3.3}$$

In addition to that, we request that the leptons fall in between the two tagging jets

$$\min\{y_{j_1}, y_{j_2}\} < y_\ell < \max\{y_{j_1}, y_{j_2}\}\,. \tag{3.4}$$

Furthermore the two same-flavor opposite-charge leptons have to be close to the on-shell mass of the Z boson,

$$66 \text{ GeV} < m_{\ell\ell} < 116 \text{ GeV}\,. \tag{3.5}$$

Because of the low mass of the Higgs boson and its very narrow width, this last cut ensures that contributions with an intermediate Higgs resonance are suppressed very strongly.

The inclusive cross section for VBF $e^+e^-\mu^+\mu^- jj$ production after applying the cuts of eqs. (3.1)–(3.5) is given by $\sigma_{ZZ}^{\text{VBF}} = 0.03003(7)$ fb at NLO in QCD and $\sigma_{ZZ}^{\text{VBF}} = 0.03249(4)$ fb at LO, where the uncertainties quoted are purely statistical. We then match the NLO calculation with the parton-shower program PYTHIA 6.4.25 [32] via POWHEG (NLO+PS). The parton shower is run with the Perugia 0 tune, including hadronization corrections, multi-parton interactions and underlying events. We do not take QED radiation effects into account. At the NLO+PS level, we obtain an inclusive cross section of $\sigma_{ZZ}^{\text{VBF}} = 0.03084(7)$ fb. In order to estimate the theoretical uncertainty of the calculation we have varied the renormalization and factorization scales in the range $m_Z/2$ to $2m_Z$, finding a change in the NLO+PS cross section between -0.0005 fb and $+0.0001$ fb which is less than 3%.

JHEP03(2014)141

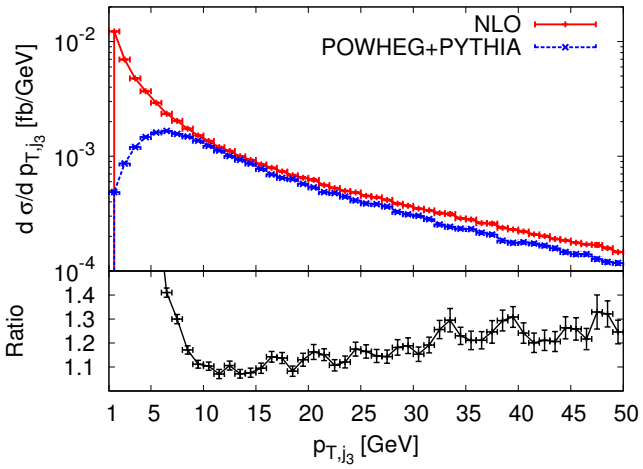

Figure 3. Transverse momentum distribution of the third jet for $pp \to e^+e^-\mu^+\mu^- jj$ at the LHC with $\sqrt{s} = 14$ TeV within the cuts of eqs. (3.1)–(3.5), at NLO (red) and at `NLO+PS` level (blue). The lower panel shows the ratio between NLO and `NLO-PS`.

Figure 2 shows the transverse momentum distributions of the hardest jet and the hardest lepton, respectively. The NLO and the `NLO+PS` results agree very well for these two observables. In general, distributions involving leptons or any of the two hardest jets are only marginally distorted by the parton-shower. We notice only a small increase in the VBF cross section by 3% when going from NLO to `NLO+PS`. This is comparable to the size of the scale variation uncertainty. Illustrated in figure 3 is the effect of the parton-shower on the transverse momentum of the third jet. In the NLO-QCD calculation for $pp \to ZZjj$ a third jet is described only at lowest non-vanishing order, as it solely arises via the real-emission contributions. When merged with the parton shower the soft-collinear radiation is resummed at leading-logarithmic accuracy via the Sudakov form factor, which results in the p_{T,j_3} distribution being damped at low transverse momentum. At higher transverse momentum we observe that the parton shower tends to slightly soften the spectrum of the third jet. The parton shower also affects the rapidity of the third jet, giving rise to an increased central jet activity. This is expected since soft QCD radiation tends to populate the central region. In figure 4 the rapidity of the third jet is shown with two different transverse-momentum cuts. Increasing the cut from 10 GeV to 20 GeV decreases the central jet activity of the parton shower without having any significant impact on the shape of the distribution at fixed order.

Instead of considering the absolute position of the third jet it can be useful to look at its relative position with respect to the two hardest jets. This is usually measured through the y^* quantity,

$$y^* = y_{j_3} - \frac{y_{j_1} + y_{j_2}}{2}. \tag{3.6}$$

Figure 5 shows that the parton shower populates the region where y^* is close to zero. This comes as no surprise, as we require the two hardest jets to be in opposite hemispheres and with a very large rapidity gap, and hence small values of y^* will often coincide with a very

JHEP03(2014)141

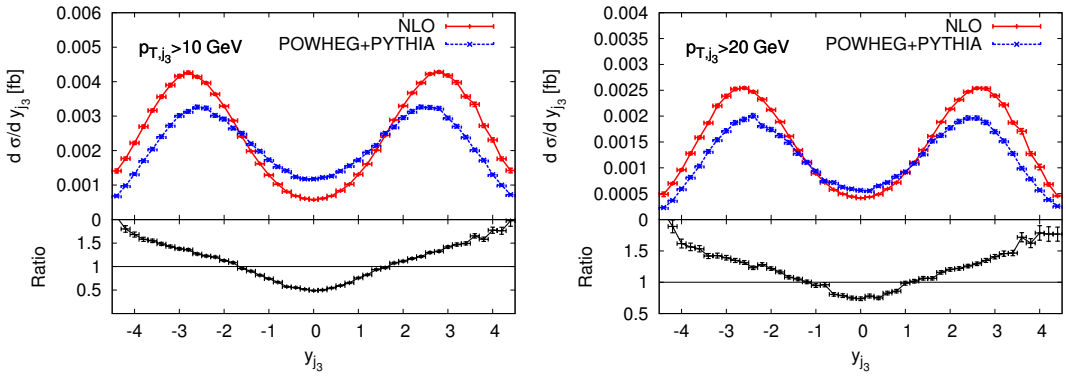

Figure 4. Rapidity of the third jet for $pp \to e^+e^-\mu^+\mu^- jj$ at the LHC with $\sqrt{s} = 14$ TeV within the cuts of eqs. (3.1)–(3.5) and a transverse momentum cut on the third jet of 10 GeV (left) and 20 GeV (right), at NLO (red) and `NLO+PS` (blue). The lower panel shows the ratio between NLO and `NLO-PS`.

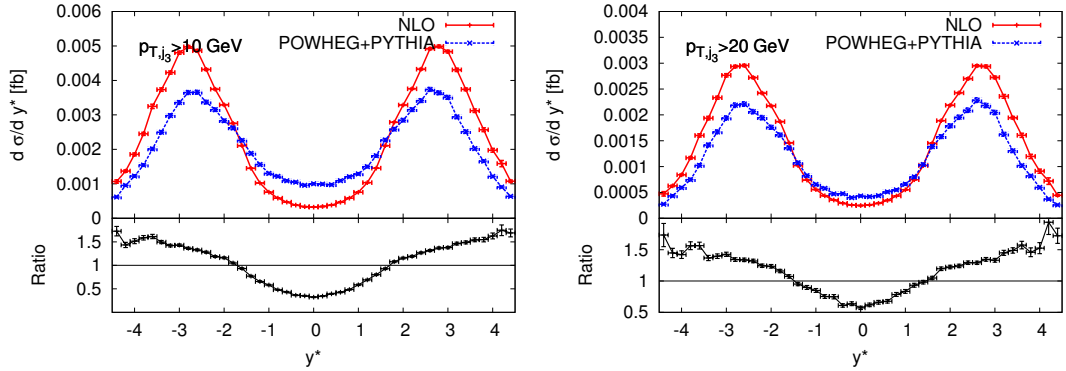

Figure 5. y^* as defined in eq. (3.6) for $pp \to e^+e^-\mu^+\mu^- jj$ at the LHC with $\sqrt{s} = 14$ TeV within the cuts of eqs. (3.1)–(3.5) and a transverse momentum cut on the third jet of 10 GeV (left) and 20 GeV (right), at NLO (red) and `NLO+PS` (blue). The lower panel shows the ratio between NLO and `NLO-PS`.

central third jet. If we increase the cut on the transverse momentum of the third jet, we again see that the effect of the parton shower is minimized.

In fact, and not surprisingly, the parton-shower has very much the same impact on the distributions involving the third jet as was reported in [18] for VBF $W^+W^- jj$.

3.2 Effective theory results

Vector boson scattering processes offer an excellent testbed for the electroweak sector at the TeV scale. A convenient way to parametrize deviations from the Standard Model is through anomalous couplings or, alternatively, an effective field theory expansion. Such an effective theory is constructed as the low-energy approximation of a more fundamental theory, and is valid up to an energy scale Λ. The explicit dependence of predictions on the scale Λ can be used to put limits on the scale of new physics itself. For scales Λ much larger than the electroweak scale we can restrict ourselves to the first correction to the SM contributions with operators of dimension six.

JHEP03(2014)141

The Lagrangian of the effective field theory can be written in the form [19]

$$\mathcal{L}_{\text{eff}} = \sum_{i,d} \frac{c_i^{(d)}}{\Lambda^{d-4}} \mathcal{O}_i^{(d)} = \mathcal{L}_{\text{SM}} + \sum_i \frac{c_i^{(6)}}{\Lambda^2} \mathcal{O}_i^{(6)} + \dots , \tag{3.7}$$

where d is the dimension of the operators $\mathcal{O}_i^{(d)}$, and the $c_i^{(d)}$ denote the coefficients of the expansion. For ease of notation we therefore drop the superscript $d = 6$ in the following.

For our analysis of VBF $ZZjj$ production we include the three CP-conserving dimension-six operators [19, 33, 34],

$$\mathcal{O}_{WWW} = \text{Tr}[W_{\mu\nu} W^{\nu\rho} W_\rho^\mu] , \tag{3.8}$$

$$\mathcal{O}_W = (D_\mu \Phi)^\dagger W^{\mu\nu} (D_\nu \Phi) , \tag{3.9}$$

$$\mathcal{O}_B = (D_\mu \Phi)^\dagger B^{\mu\nu} (D_\nu \Phi) , \tag{3.10}$$

and the two CP-violating operators ,

$$\mathcal{O}_{\tilde{W}WW} = \text{Tr}[\tilde{W}_{\mu\nu} W^{\nu\rho} W_\rho^\mu] , \tag{3.11}$$

$$\mathcal{O}_{\tilde{W}} = (D_\mu \Phi)^\dagger \tilde{W}^{\mu\nu} (D_\nu \Phi) , \tag{3.12}$$

where Φ is the Higgs doublet field, and

$$D_\mu = \partial_\mu + \frac{i}{2} g \tau^I W_\mu^I + \frac{i}{2} g' B_\mu , \tag{3.13}$$

$$W_{\mu\nu} = \frac{i}{2} g \tau^I (\partial_\mu W_\nu^I - \partial_\nu W_\mu^I + g \epsilon_{IJK} W_\mu^J W_\nu^K) , \tag{3.14}$$

$$B_{\mu\nu} = \frac{i}{2} g' (\partial_\mu B_\nu - \partial_\nu B_\mu) . \tag{3.15}$$

Here, the B^μ and W^μ denote the U(1) and SU(2) gauge fields with the associated couplings g' and g, respectively, and τ^I the weak isospin matrices. The dual field strength tensor is defined as

$$\tilde{W}_{\mu\nu} = \epsilon_{\alpha\beta\mu\nu} W^{\alpha\beta} . \tag{3.16}$$

It is worth noting that the five operators of eqs. (3.8)–(3.12) form a minimal set of operators affecting the triple and quartic gauge boson couplings. For completeness we show which weak gauge boson vertices are affected by the five operators defined above in table 1.

Our implementation of the effective Lagrangian approach for VBF $ZZjj$ production allows the user to specify the values of the c_i/Λ^2 in units of TeV^{-2} for each of the operators of eqs. (3.8)–(3.12). Here, we will show the effect of the two operators $\mathcal{O}_{WWW}$ and $\mathcal{O}_{\tilde{W}WW}$ for values of c_{WWW}/Λ^2 and $c_{\tilde{W}WW}/\Lambda^2$ consistent with current limits on the anomalous couplings λ_Z and $\tilde{\lambda}_Z$. These can be transformed into limits on effective field theory parameters through a set of tree-level relations. However, the relations between the anomalous couplings and the effective field theory parameters are not exact, in the sense that they assume no form factor dependence and disregard contributions from higher dimensional operators.

JHEP03(2014)141

	WWZ	$WW\gamma$	WWH	ZZH	γZH	$WWWW$	$WWZZ$	$WWZ\gamma$	$WW\gamma\gamma$
$\mathcal{O}_{WWW}$	×	x	—	—	—	×	x	×	x
$\mathcal{O}_{W}$	×	x	×	x	×	x	×	x	—
$\mathcal{O}_{B}$	×	x	—	×	x	—	—	—	—
$\mathcal{O}_{\tilde{W}WW}$	×	x	—	—	—	×	x	×	x
$\mathcal{O}_{\tilde{W}}$	×	x	×	x	×	—	—	—	—

Table 1. Crosses indicate triple and quartic weak boson vertices affected by the dimension-six operators of eqs. (3.8)–(3.12). Taken from ref. [34].

From [33, 35] we have

$$\frac{c_{WWW}}{\Lambda^2} = \frac{2}{3g^2 m_W^2}\lambda_Z\,, \tag{3.17}$$

$$\frac{c_{\tilde{W}WW}}{\Lambda^2} = \frac{1}{3g^2 m_W^2}\tilde{\lambda}_Z\,, \tag{3.18}$$

which translates into

$$-11.9\ \text{TeV}^{-2} < \frac{c_{WWW}}{\Lambda^2} < -1.94\ \text{TeV}^{-2}\,, \tag{3.19}$$

$$-19.4\ \text{TeV}^{-2} < \frac{c_{\tilde{W}WW}}{\Lambda^2} < -2.42\ \text{TeV}^{-2}\,, \tag{3.20}$$

when using the current combined limits of [36] at the 68% confidence level. The limits become compatible with the Standard Model at the 95% confidence level.

Our setup is identical to that of section 3.1, except we choose running factorization and renormalization scales,

$$\mu_R = \mu_F = \frac{\sqrt{M_Z^2 + p_{T,Z_1}^2} + \sqrt{M_Z^2 + p_{T,Z_2}^2} + \sum_i p_{T,i}}{2}\,, \tag{3.21}$$

where the $p_{T,i}$ are the transverse momenta of the (two or three) final state partons and the p_{T,Z_i} the transverse momenta of a same-type lepton pair. Such a dynamical scale is expected to optimally account for the high-transverse momentum region where the effective operators have the largest impact.

Our analysis within the effective field theory approach is done in analogy to the SM analysis of section 3.1. We present results obtained for the $\ell^+\ell^-\ell'^+\ell'^-$ decay mode within the cuts of eqs. (3.1)–(3.5). We account for decays into any combination of electrons and muons by multiplying results obtained for the $e^+e^-\mu^+\mu^-$ decay mode by a factor of two. As mentioned earlier this procedure neglects any interference effects for the leptons. In order to illustrate the effect dimension-six operators can have on observables we consider the operators $\mathcal{O}_{WWW}$ and $\mathcal{O}_{\tilde{W}WW}$ independently by setting the associated expansion coefficients to values compatible with the current experimental bounds of eqs. (3.19) and (3.20), and all other to zero. To this end, we separately choose $c_{WWW}/\Lambda^2 = -5\ \text{TeV}^{-2}$ and $c_{\tilde{W}WW}/\Lambda^2 = -5\ \text{TeV}^{-2}$. In diagrams where more than one vertex could be affected by the

JHEP03(2014)141

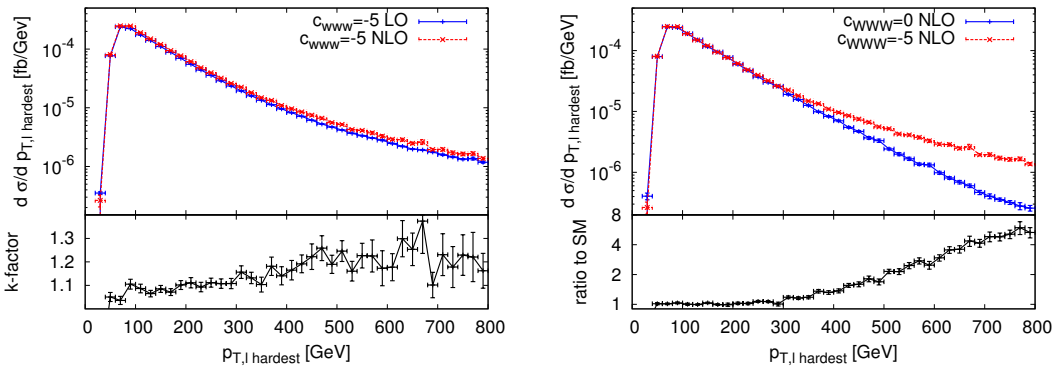

Figure 6. Transverse momentum distribution of the hardest lepton for $pp \to e^+e^-\mu^+\mu^-jj$ at the LHC with $\sqrt{s} = 14$ TeV within the cuts of eqs. (3.1)–(3.5), with $c_{WWW}/\Lambda^2 = -5$ TeV^{-2} at LO and NLO (left panel), and at NLO with $c_{WWW}/\Lambda^2 = -5$ TeV^{-2} and $c_{WWW}/\Lambda^2 = 0$ (right panel). The lower panels show the respective ratios.

effective operator, we only turn on the effective coupling for one vertex at a time. This is consistent with only considering dimension six operators, as diagrams suppressed by more than one factor of Λ^{-2} should also receive corrections from operators of higher dimension. Because of the explicit scale suppression of the effective operators, it is expected that deviations from the Standard Model are most easily seen in the tails of differential distributions that are sensitive to the high-energy regime. From our SM analysis of section 3.1 we may conclude that a parton shower has very little effect on the distributions that do not involve the third jet. In this section we therefore only discuss fixed-order results. In figure 6 (left panel) we show the transverse mass distribution of the hardest lepton at LO and NLO for $c_{WWW}/\Lambda^2 = -5$ TeV^{-2} together with the associated dynamical K-factor, defined by

$$K(x) = \frac{d\sigma_{NLO}/dx}{d\sigma_{LO}/dx}\,, \tag{3.22}$$

and a comparison of the NLO prediction for $c_{WWW}/\Lambda^2 = -5$ TeV^{-2} with the SM result (right panel). All other dimension-six operator coefficients are set to zero. We note that the impact of the NLO-QCD corrections and the considered dimension-six operator contributions is of the same order of magnitude in the range of low to intermediate transverse momenta. For smaller absolute values of c_{WWW}/Λ^2 the NLO corrections are significant up to even higher transverse momenta. Hence, in that case, in order to unambiguously distinguish new physics from higher-order perturbative effects in the Standard Model, full NLO-QCD results have to be considered.

When fixing $c_{WWW} = c_{\tilde{W}WW}$ one notices that the CP-violating operator $\mathcal{O}_{\tilde{W}WW}$ yields an enhancement in the tails of the transverse momentum distribution of the hardest lepton that is larger by roughly a factor two, c. f. figure 7. This is due to the normalization chosen in eq. (3.16), which would be more naturally defined with a factor 1/2 on the right-hand-side. Qualitatively similar results are obtained for the invariant mass of the four-lepton system, as illustrated by figure 8.

In order to estimate how sensitive the LHC is to the two couplings c_{WWW}/Λ^2 and $c_{\tilde{W}WW}/\Lambda^2$ we have computed the number of events in the tail of the transverse momentum distribution of the hardest lepton, $p_{T,\ell}^{\text{hardest}} > 340$ GeV, for the Standard Model, for

JHEP03(2014)141

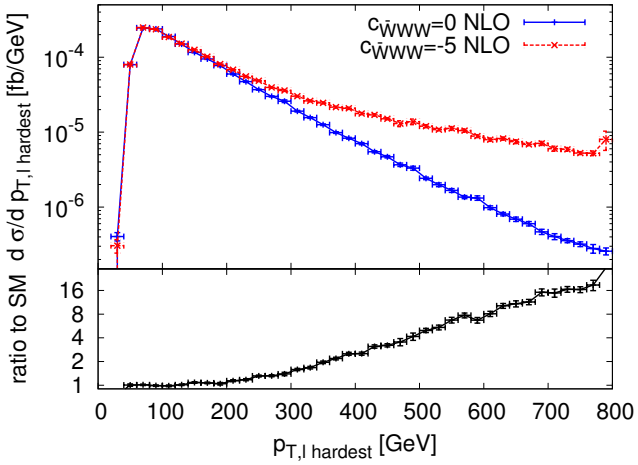

Figure 7. Transverse momentum distribution of the hardest lepton for $pp \to e^+e^-\mu^+\mu^- jj$ at the LHC with $\sqrt{s} = 14$ TeV within the cuts of eqs. (3.1)–(3.5), at NLO with $c_{\tilde{W}WW}/\Lambda^2 = -5$ TeV^{-2} and $c_{\tilde{W}WW}/\Lambda^2 = 0$, together with the respective ratio.

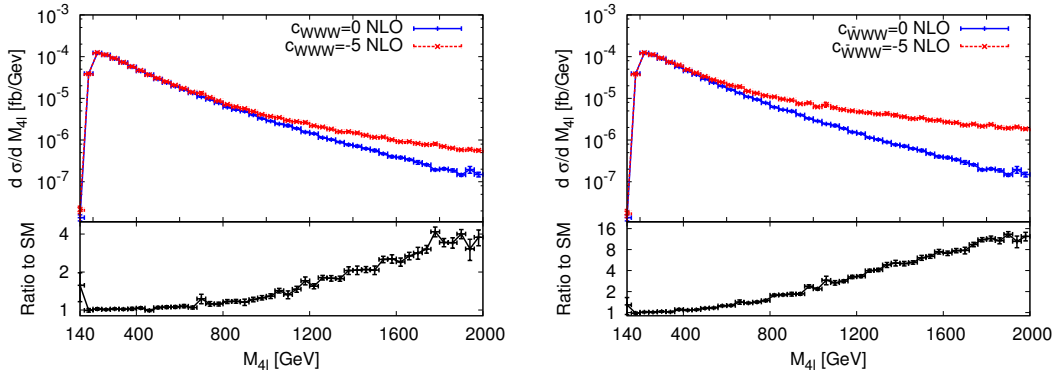

Figure 8. Invariant mass distribution of the four-lepton system in $pp \to e^+e^-\mu^+\mu^- jj$ at the LHC with $\sqrt{s} = 14$ TeV within the cuts of eqs. (3.1)–(3.5), at NLO with $c_{WWW}/\Lambda^2 = -5$ TeV^{-2} and $c_{WWW}/\Lambda^2 = 0$ (left), $c_{\tilde{W}WW}/\Lambda^2 = -5$ TeV^{-2} and $c_{\tilde{W}WW}/\Lambda^2 = 0$ (right), together with the respective ratio.

$c_{WWW}/\Lambda^2 = -5$ TeV^{-2} and for $c_{\tilde{W}WW}/\Lambda^2 = -5$ TeV^{-2}, respectively, with integrated luminosities of 300 fb^{-1} and 3000 fb^{-1}, c. f. table 2. The cut-off value of 340 GeV is chosen upon inspection of the transverse-momentum distributions, where we start observing a significant deviation from the Standard Model around this region, c. f. figures 6 and 7. We note that for different values of c_{WWW}/Λ^2 and $c_{\tilde{W}WW}/\Lambda^2$, we would find different values for the cut-off. For consistency we will use $p_{T,\ell}^{\text{hardest}} = 340$ GeV as cut-off for all values of c_{WWW}/Λ^2 and $c_{\tilde{W}WW}/\Lambda^2$.

The significance of a non-Standard Model (nSM) signal is defined via the number of events in the nSM and the SM scenarios as

$$\frac{|\#\,\text{events(nSM)} - \#\,\text{events(SM)}|}{\sqrt{\#\,\text{events(SM)}}}\,. \tag{3.23}$$

Assuming that events are distributed according to a Gaussian distribution, a one-, two- and

JHEP03(2014)141

	events @ 300 fb^{-1}	significance	events @ 3000 fb^{-1}	significance
SM	0.692	—	6.92	—
$\frac{c_{WWW}}{\Lambda^2} = -5$ TeV^{-2}	1.49	0.96	14.9	3.0
$\frac{c_{\tilde{W}WW}}{\Lambda^2} = -5$ TeV^{-2}	3.76	3.7	37.6	11.64

Table 2. Number of events for $pp \to \ell^+\ell^-\ell'^+\ell'^- jj$ at NLO-QCD at the LHC with $\sqrt{s} = 14$ TeV within the cuts of eqs. (3.1)–(3.5) and an additional cut of $p_{T,\ell}^{\text{hardest}} > 340$ GeV, together with the significance of the signal defined in eq. (3.23).

	events @ 300 fb^{-1}	significance	events @ 3000 fb^{-1}	significance
SM	0.599	—	5.99	—
$\frac{c_{WWW}}{\Lambda^2} = -5$ TeV^{-2}	1.22	0.80	12.2	2.5
$\frac{c_{\tilde{W}WW}}{\Lambda^2} = -5$ TeV^{-2}	3.03	3.1	30.3	9.9

Table 3. Same as table 2, but at LO.

$\frac{c_{WWW}}{\Lambda^2}$	events @ 14 TeV	significance	events @ 33 TeV	significance	events @ 100 TeV	significance
0.0 TeV^{-2}	0.200	—	3.26	—	32.1	—
-2.0 TeV^{-2}	0.234	0.0765	4.47	0.671	74.6	7.51
-4.0 TeV^{-2}	0.334	0.301	8.12	2.70	203	30.2
-6.0 TeV^{-2}	0.496	0.663	14.3	6.10	419	68.3
-8.0 TeV^{-2}	0.725	1.18	22.8	10.8	720	122
-10.0 TeV^{-2}	1.01	1.82	33.7	16.9	1110	190

Table 4. Number of events for $pp \to \ell^+\ell^-\ell'^+\ell'^- jj$ for different collider energies with an integrated luminosity 100 fb^{-1}, within the cuts of eqs. (3.1)–(3.5) and an additional cut of $p_{T,\ell}^{\text{hardest}} > 340$ GeV in the SM and including the effect of $\mathcal{O}_{WWW}$, together with the significance of the signal defined in eq. (3.23).

three-sigma significance correspond to the well-known 68%, 95% and 99.8% probabilities. When the expected number of SM events is low, one needs however to bear in mind that events are distributed according to a Poisson distribution. In this case these significances correspond to lower probabilities. When the expected number of SM events is however larger than five, we find that these probabilities differ already by less than 1%.

Already at 300 fb^{-1} the dimension-six operators result in a significant signal for the CP-violating coupling. However, in the high-luminosity phase of the LHC with 3000 fb^{-1}, CP-conserving operators with $c_{WWW}/\Lambda^2 = -5$ TeV^{-2} become significant at the three sigma level and CP-violating operators with $c_{\tilde{W}WW}/\Lambda^2 = -5$ TeV^{-2} are significant to more than five sigma.

It is worth noting that the significance decreases, if only LO results are taken into account. Comparing tables 2 and 3 we observe that the significance increases by $\sim 20\%$, when NLO-QCD corrections are included. This strongly favors including the NLO-QCD corrections, as a similar gain in significance by technical means would require an increase in luminosity of $\sim 44\%$.

JHEP03(2014)141

$\frac{c_{\tilde{W}WW}}{\Lambda^2}$	events @ 14 TeV	significance	events @ 33 TeV	significance	events @ 100 TeV	significance
0.0 TeV^{-2}	0.200	—	3.26	—	32.1	—
−2.0 TeV^{-2}	0.331	0.293	8.12	2.70	205	30.3
−4.0 TeV^{-2}	0.717	1.16	22.8	10.9	723	121
−6.0 TeV^{-2}	1.36	2.60	47.3	24.4	1580	272
−8.0 TeV^{-2}	2.27	4.64	81.7	43.5	2790	484
−10.0 TeV^{-2}	3.43	7.23	125	67.7	4350	759

Table 5. Same as table 4, but including the operator $\mathcal{O}_{\tilde{W}WW}$.

If we consider only contributions of one operator, e.g. $\mathcal{O}_{WWW}$, the matrix element squared schematically takes the form

$$|\mathcal{M}|^2 = |\mathcal{M}_{SM}|^2 + \frac{c_{WWW}^2}{\Lambda^4}|\tilde{\mathcal{M}}_{WWW}|^2 + \frac{c_{WWW}}{\Lambda^2}(\tilde{\mathcal{M}}_{WWW}\mathcal{M}_{SM}^* + \mathcal{M}_{SM}\tilde{\mathcal{M}}_{WWW}^*)\,. \tag{3.24}$$

By calculating the cross section for at least three different values of the coupling c_{WWW}/Λ^2 (or $c_{\tilde{W}WW}/\Lambda^2$) it is possible to interpolate the cross section for any value of the coupling. Using this, we expect the following one sigma bounds for the LHC at 300 fb^{-1},

$$-4.98 \text{ TeV}^{-2} < \frac{c_{WWW}}{\Lambda^2} < 5.12 \text{ TeV}^{-2}\,, \tag{3.25}$$

$$-2.54 \text{ TeV}^{-2} < \frac{c_{\tilde{W}WW}}{\Lambda^2} < 2.54 \text{ TeV}^{-2}\,, \tag{3.26}$$

and at 3000 fb^{-1},

$$-2.77 \text{ TeV}^{-2} < \frac{c_{WWW}}{\Lambda^2} < 2.91 \text{ TeV}^{-2}\,, \tag{3.27}$$

$$-1.43 \text{ TeV}^{-2} < \frac{c_{\tilde{W}WW}}{\Lambda^2} < 1.43 \text{ TeV}^{-2}\,. \tag{3.28}$$

We see that these limits are already tighter than the current experimental limits quoted in eqs. (3.19)–(3.20). Note that the limits only improve by a factor $10^{1/4} \sim 1.8$ when the luminosity is increased by a factor of 10. This is related to the fact that for large values of c_{WWW}/Λ^2 we are essentially only probing c_{WWW}^2/Λ^4, see eq. (3.24). The limits on the coupling improve then with a quartic root of the available luminosity.

Even better significances could be obtained with hadron colliders operating at higher energies, such as the high-energy upgrade of the LHC (HE-LHC) with an energy of $\sqrt{s} = 33\,\text{TeV}$, or a future VLHC with an energy of up to $\sqrt{s} = 100\,\text{TeV}$. Tables 4 and 5 show expected numbers of events and associated significances for various scenarios at the LHC, HE-LHC and VLHC at LO. As reported above the significance is expected to increase at NLO QCD.

Depending on the luminosity delivered, already for rather small values of the operator coefficient c_{WWW}/Λ^2 an excess over the SM values should be visible. Here we observe that the significances grow faster than the collider energy squared.

To better illustrate the impact of increasing energy and integrated luminosity, we have plotted the significance of a signal as a function of the value of the coupling and the

JHEP03(2014)141

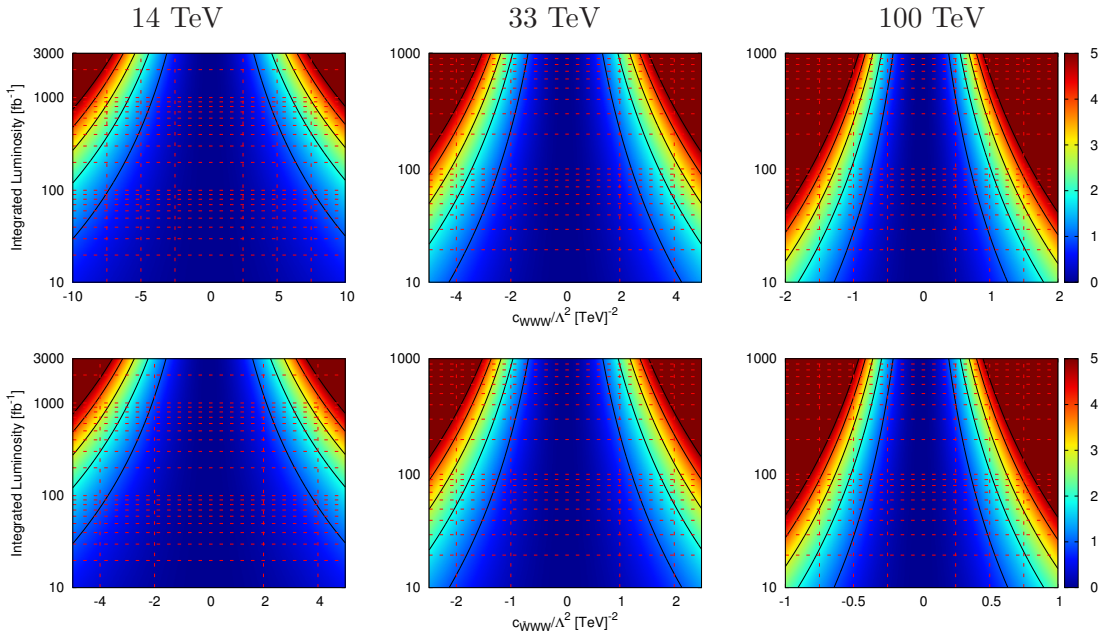

Figure 9. Significance of the two couplings c_{WWW}/Λ^2 and $c_{\tilde{W}WW}/\Lambda^2$ for the process $pp \to \ell^+\ell^-\ell'^+\ell'^-jj$ at 14 TeV, 33 TeV and 100 TeV within the cuts of eqs. (3.1)–(3.5) and $p_{T,\ell}^{\text{hardest}} > 340$ GeV, as a function of the integrated luminosity. The five black lines indicate one, two, three, four and five sigma significance defined in eq. (3.23), corresponding to the color code indicated on the right-hand-side.

integrated luminosity for each of the energies 14 TeV, 33 TeV, and 100 TeV in figure 9. It is obvious from these plots that in order to improve the current limits on anomalous couplings, higher energy is much more useful than higher luminosity.

It should be noted that we have disregarded the effects of various reducible and irreducible background processes, e.g. QCD-induced $ZZjj$ production, which would increase the SM contribution by about 50% within our setup. A realistic assessment of the full significances would require to include these backgrounds, as well as additional uncertainties, such as experimental efficiencies, mis-identification issues, etc. It is outside the scope of the present work to systematically account for these effects.

4 Conclusions

In this work, we have presented an implementation of electroweak $ZZjj$ production in the `POWHEG BOX V2`, a framework for the matching of NLO-QCD calculations with parton-shower programs. We take non-resonant contributions, off-shell effects and spin correlations of the final-state particles into account. In the context of the Standard Model, we have considered the leptonic and semi-leptonic decay modes of the Z bosons. In addition, effects of new physics in the gauge-boson sector that arise from an effective Lagrangian with operators up to dimension six have been implemented. The code we have developed is publicly available from the webpage of the `POWHEG BOX` project, http://powhegbox.mib.infn.it/.

JHEP03(2014)141

Here, we have discussed results for two specific scenarios. First, we have performed a numerical analysis of Standard-Model $e^+e^-\mu^+\mu^-jj$ production at the LHC with $\sqrt{s} = 14\,\text{TeV}$, in the regime where both Z bosons are close to on-shell. In this setup, the impact of the parton shower is small for most observables related to the hard leptons and tagging jets, while larger effects are observed in distributions related to an extra jet. Second, we have considered an effective field theory with operators of up to dimension six, and explored the impact of such operators on observables in VBF $ZZjj$ processes. We found that tails of transverse-momentum and invariant mass distributions of the hard jets and leptons are most sensitive to such new-physics contributions. Since the statistical significance of $ZZjj$ results at the LHC with an energy of $\sqrt{s} = 14\,\text{TeV}$ and an integrated luminosity of about $300\,\text{fb}^{-1}$ is limited, we additionally explored scenarios for high-energy proton colliders, such as an HE-LHC and a VLHC, with collider energies of 33 TeV and 100 TeV, respectively. We found that an increase in energy would help, much more than an increase in luminosity, to substantially improve current limits on anomalous couplings in the gauge boson sector. For instance, an improvement in significance by a factor of four can be obtained by increasing the energy by a factor of (less than) two, or by increasing the luminosity by a factor of 16. We also note that, for the process we have considered, relative NLO corrections in the SM and in the effective field theory approach are of the same size. However, since in the effective field theory scenario the number of events in tails of transverse-momentum distributions is larger than in the SM, the NLO corrections increase the significance by the square root of the K factor, see eq. (3.23). This, together with the well-known fact that uncertainties are reduced significantly at NLO, strongly supports the use of NLO simulations in the context of searches for new physics in the gauge-boson sector.

Acknowledgments

We are grateful to Celine Degrande for useful comments. The work of B. J. is supported in part by the German Federal Ministry for Education and Research (BMBF). G. Z. is supported by the LHCPhenoNet network under the Grant Agreement PITN-GA-2010-264564. A. K. is supported by the British Science and Technology Facilities Council and by the Buckee Scholarship at Merton College.

References

[1] ATLAS collaboration, *Observation of a new particle in the search for the standard model Higgs boson with the ATLAS detector at the LHC*, *Phys. Lett.* **B 716** (2012) 1 [arXiv:1207.7214] [INSPIRE].

[2] CMS collaboration, *Observation of a new boson at a mass of* 125 *GeV with the CMS experiment at the LHC*, *Phys. Lett.* **B 716** (2012) 30 [arXiv:1207.7235] [INSPIRE].

JHEP03(2014)141

[3] ATLAS collaboration, *Evidence for the spin-0 nature of the Higgs boson using ATLAS data*, *Phys. Lett.* **B 726** (2013) 120 [arXiv:1307.1432] [INSPIRE].

[4] CMS collaboration, *Study of the mass and spin-parity of the Higgs boson candidate via its decays to Z boson pairs*, *Phys. Rev. Lett.* **110** (2013) 081803 [arXiv:1212.6639] [INSPIRE].

[5] D. Zeppenfeld, R. Kinnunen, A. Nikitenko and E. Richter-Was, *Measuring Higgs boson couplings at the CERN LHC*, *Phys. Rev.* **D 62** (2000) 013009 [hep-ph/0002036] [INSPIRE].

[6] M. Dührssen et al., *Extracting Higgs boson couplings from CERN LHC data*, *Phys. Rev.* **D 70** (2004) 113009 [hep-ph/0406323] [INSPIRE].

[7] LHC Higgs Cross Section Working Group collaboration, A. David et al., *LHC HXSWG interim recommendations to explore the coupling structure of a Higgs-like particle*, arXiv:1209.0040 [INSPIRE].

[8] B. Jager, C. Oleari and D. Zeppenfeld, *Next-to-leading order QCD corrections to Z boson pair production via vector-boson fusion*, *Phys. Rev.* **D 73** (2006) 113006 [hep-ph/0604200] [INSPIRE].

[9] K. Arnold et al., *VBFNLO: a parton level Monte Carlo for processes with electroweak bosons*, *Comput. Phys. Commun.* **180** (2009) 1661 [arXiv:0811.4559] [INSPIRE].

[10] K. Arnold et al., *VBFNLO: a parton level Monte Carlo for processes with electroweak bosons – Manual for version 2.5.0*, arXiv:1107.4038 [INSPIRE].

[11] K. Arnold et al., *Release note — Vbfnlo-2.6.0*, arXiv:1207.4975 [INSPIRE].

[12] P. Nason, *A new method for combining NLO QCD with shower Monte Carlo algorithms*, *JHEP* **11** (2004) 040 [hep-ph/0409146] [INSPIRE].

[13] S. Frixione, P. Nason and C. Oleari, *Matching NLO QCD computations with parton shower simulations: the POWHEG method*, *JHEP* **11** (2007) 070 [arXiv:0709.2092] [INSPIRE].

[14] S. Alioli, P. Nason, C. Oleari and E. Re, *A general framework for implementing NLO calculations in shower Monte Carlo programs: the POWHEG BOX*, *JHEP* **06** (2010) 043 [arXiv:1002.2581] [INSPIRE].

[15] J.M. Campbell, R.K. Ellis, P. Nason and G. Zanderighi, *W and Z bosons in association with two jets using the POWHEG method*, *JHEP* **08** (2013) 005 [arXiv:1303.5447] [INSPIRE].

[16] B. Jäger, S. Schneider and G. Zanderighi, *Next-to-leading order QCD corrections to electroweak Zjj production in the POWHEG BOX*, *JHEP* **09** (2012) 083 [arXiv:1207.2626] [INSPIRE].

[17] B. Jager and G. Zanderighi, *NLO corrections to electroweak and QCD production of W^+W^+ plus two jets in the POWHEGBOX*, *JHEP* **11** (2011) 055 [arXiv:1108.0864] [INSPIRE].

[18] B. Jager and G. Zanderighi, *Electroweak W^+W^-jj prodution at NLO in QCD matched with parton shower in the POWHEG-BOX*, *JHEP* **04** (2013) 024 [arXiv:1301.1695] [INSPIRE].

[19] C. Degrande et al., *Effective field theory: a modern approach to anomalous couplings*, *Annals Phys.* **335** (2013) 21 [arXiv:1205.4231] [INSPIRE].

[20] J. Alwall, M. Herquet, F. Maltoni, O. Mattelaer and T. Stelzer, *MadGraph 5: going beyond*, *JHEP* **06** (2011) 128 [arXiv:1106.0522] [INSPIRE].

[21] A. Denner, L. Hosekova and S. Kallweit, *NLO QCD corrections to W^+W^+jj production in vector-boson fusion at the LHC*, *Phys. Rev.* **D 86** (2012) 114014 [arXiv:1209.2389] [INSPIRE].

JHEP03(2014)141

[22] T. Melia, P. Nason, R. Rontsch and G. Zanderighi, *W^+W^-, WZ and ZZ production in the POWHEG BOX*, *JHEP* **11** (2011) 078 [arXiv:1107.5051] [INSPIRE].

[23] A. Altheimer et al., *Boosted objects and jet substructure at the LHC*, arXiv:1311.2708 [INSPIRE].

[24] A. Martin, W. Stirling, R. Thorne and G. Watt, *Parton distributions for the LHC*, *Eur. Phys. J.* **C 63** (2009) 189 [arXiv:0901.0002] [INSPIRE].

[25] M. Whalley, D. Bourilkov and R. Group, *The Les Houches accord PDFs (LHAPDF) and LHAGLUE*, hep-ph/0508110 [INSPIRE].

[26] M. Cacciari and G.P. Salam, *Dispelling the N^3 myth for the k_t jet-finder*, *Phys. Lett.* **B 641** (2006) 57 [hep-ph/0512210] [INSPIRE].

[27] M. Cacciari, G.P. Salam and G. Soyez, *The anti-k_t jet clustering algorithm*, *JHEP* **04** (2008) 063 [arXiv:0802.1189] [INSPIRE].

[28] M. Cacciari, G.P. Salam and G. Soyez, *FastJet user manual*, *Eur. Phys. J.* **C 72** (2012) 1896 [arXiv:1111.6097] [INSPIRE].

[29] ATLAS collaboration, *Measurement of ZZ production in pp collisions at $\sqrt{s} = 7$ TeV and limits on anomalous ZZZ and $ZZ\gamma$ couplings with the ATLAS detector*, *JHEP* **03** (2013) 128 [arXiv:1211.6096] [INSPIRE].

[30] D.L. Rainwater, R. Szalapski and D. Zeppenfeld, *Probing color singlet exchange in Z + two jet events at the CERN LHC*, *Phys. Rev.* **D 54** (1996) 6680 [hep-ph/9605444] [INSPIRE].

[31] D.L. Rainwater and D. Zeppenfeld, *Observing $H \to W^*W^* \to e^\pm\mu^\mp \not{p}_T$ in weak boson fusion with dual forward jet tagging at the CERN LHC*, *Phys. Rev.* **D 60** (1999) 113004 [*Erratum ibid.* **D 61** (2000) 099901] [hep-ph/9906218] [INSPIRE].

[32] T. Sjöstrand, S. Mrenna and P.Z. Skands, *PYTHIA 6.4 physics and manual*, *JHEP* **05** (2006) 026 [hep-ph/0603175] [INSPIRE].

[33] K. Hagiwara, S. Ishihara, R. Szalapski and D. Zeppenfeld, *Low-energy effects of new interactions in the electroweak boson sector*, *Phys. Rev.* **D 48** (1993) 2182 [INSPIRE].

[34] C. Degrande et al., *Monte Carlo tools for studies of non-standard electroweak gauge boson interactions in multi-boson processes: a Snowmass white paper*, arXiv:1309.7890 [INSPIRE].

[35] J. Wudka, *Electroweak effective Lagrangians*, *Int. J. Mod. Phys.* **A 9** (1994) 2301 [hep-ph/9406205] [INSPIRE].

[36] Particle Data Group collaboration, J. Beringer et al., *Review of particle physics*, *Phys. Rev.* **D 86** (2012) 010001 [INSPIRE].

JHEP03(2014)141